Available online at www.sciencedirect.com
SCIENCE DIRECT
Journal of Catalysis 241 (2006) 103–114
JOURNAL OF CATALYSIS
www.elsevier.com/locate/jcat

Identity and location of active species for NO reduction by CH_4 over Co-ZSM-5

C. Chupin, A.C. van Veen, M. Konduru, J. Després, C. Mirodatos *

Institut de Recherches sur la Catalyse (CNRS UPR 5401), 2 av. A. Einstein, F-69626 Villeurbanne cedex, France

Received 12 December 2005; revised 4 April 2006; accepted 6 April 2006

Available online 30 May 2006

Abstract

Cobalt-exchanged zeolite samples were characterized using XRD, XPS, TEM, and UV–vis spectroscopy. Co-ZSM-5 of varying exchange degree was prepared by ion-exchange of H-ZSM-5 with cobalt acetate. Three different species were observed: (i) Co^{2+} cations located at α and β sites in the zeolite channels, (ii) microaggregates composed of cobalt and oxygen, and (iii) cobalt oxide particles of type CoO and CO_3O_4, including cobalt silicate for overexchanged samples. The formation of microaggregates proceeded through clustering of hydrated Co^{2+} cations located at α sites. Their size indicates that they are located at the intersection of the zeolite channels. Further clustering of those microaggregates in the presence of water led to the formation of cobalt oxide particles located at defect sites or at the outer surface of the zeolite grains. The microaggregates were found to be active species in the reduction of NO to N_2 using methane as the reducing agent. Larger outer oxide/silicate species were involved mainly in unselective parallel combustion reactions. In contrast, the isolated cobalt cations acted predominantly as adsorption sites for NO. Aging experiments in the presence of water and sulfur dioxide demonstrated a decline in activity by ca. 20% before a constant conversion was reached. The irreversible deactivation can be explained by a weakening of the interaction between cobalt internal clusters and zeolite hydroxyl groups.

Keywords: NO reduction in the presence of methane; Selective catalytic reduction on Co-ZSM-5; Cobalt active; Selective and non-selective species

1. Introduction

Emission of nitrogen oxides from stationary and mobile sources is a major issue facing industrialized nations. Catalytic processes achieve satisfactory levels of NO_x abatement. They are based on the reduction of nitrogen oxides to dinitrogen using hydrocarbons [1] or ammonia [2,3] as reducing agents. The best catalyst choice for a given application strongly depends on the reducing molecule and the operating conditions used. In the case of domestic heaters working with, for example, natural gas, the catalyst must reach a high deNO_x performance in the selective catalytic reduction of NO_x using unburned methane as a reducing agent (CH_4-SCR),

$$2NO + CH_4 + O_2 \rightarrow N_2 + CO_2 + 2H_2O. \quad (1)$$

Among the various catalyst formulations, cobalt-exchanged zeolites have shown promising activity in the selective catalytic reduction (SCR) of methane [4–6]. In fact, cobalt shows a high selectivity for the deNO_x reaction (1), whereas other metals, such as copper, are more active in the parallel reactions of combustion of the hydrocarbons [7]. Moreover, Co-ZSM-5 exhibits a good hydrothermal stability compared with the conventional copper-exchanged zeolites [8].

Co-ZSM-5 catalysts can be prepared by several methods, although ion exchange using aqueous solutions of cobalt acetate or cobalt nitrate is usually preferred over solid-state ion exchange [9] or sublimation [10]: A higher dispersion of cobalt species is achieved by the ion-exchange method. Despite considerable efforts directed at characterizing cobalt species in Co-ZSM-5 catalysts, there is an ongoing debate on the nature and role of catalytic entities. Dedecek et al. showed that Co^{2+} cations could be located at α, β, and γ sites in ZSM-5 [11]. These three different sites are located inside the main channels for the α sites, inside the sinusoidal channels for the β sites, and accessible from the sinusoidal sites for the γ sites, and thus all can be considered accessible from the gas phase. When all exchange sites are occupied by cobalt cations, forma-

* Corresponding author. Fax: +33 472 445399.
E-mail address: claude.mirodatos@catalyse.cnrs.fr (C. Mirodatos).

0021-9517/$ – see front matter
doi:10.1016/j.jcat.2006.04.025

tion of aggregates of cobalt [9,12,13], and of particles of oxides Co_2O_3, Co_3O_4, and CoO has been reported previously [14,15]. For the case of overexchanged material (e.g., Co/Al = 1.5) using cobalt acetate, the formation of cobalt phyllosilicate outside the zeolite has been reported [26].

The present paper reports the characteristics of various cobalt species formed in Co-ZSM-5 prepared by ion exchange, to be used as a quantitative basis for assigning active site coverage in mechanistic and kinetic studies [12,13,16]. The influence of the degree of exchange and of the Si/Al ratio on the Co species is investigated. The catalytic activities of the various species for the reduction of NO with CH_4 in the presence of oxygen and for the unselective parallel reactions are outlined and related to the performance of the catalytic system. The mechanisms involved in the formation of the various cobalt species are also discussed. Finally, the best formulation is tested under more severe conditions for long-term activity in the presence of water and sulfur dioxide, at concentrations fixed according the target application.

2. Experimental

2.1. Catalyst preparation

Herein Co-ZSM-5 catalysts are identified in a CoZ-xx-yyy format, with xx = Si/Al (atomic) and yyy = % degree of exchange (%DE) = $200 \times [\mathrm{Co/Al}]_{\mathrm{atomic}}$. Samples with two Si/Al atomic ratios and various exchange degrees were prepared via a conventional ion-exchange technique reported previously [13,16]. Briefly, the preparation of catalysts with Si/Al = 25 (i.e., CoZ-25-39, -60, -104, -115, and -248) involved the dissolution of a known amount of $Co(CH_3COO)_2$ (Fluka Chemicals, ⩾99%) in 750 mL of deionized water, followed by the addition of 6 g of H-ZSM-5 (Zeolyst International; Si/Al = 25, $S_{\mathrm{BET}} = 400\ \mathrm{m^2/g}$, pore volume = 0.2 mL/g). The resulting solution was continuously stirred mechanically, with the pH value maintained at 6–7. The resulting solid obtained after centrifuging was washed repeatedly with distilled water and dried in air for 12 h at 120 °C. The catalysts with a Si/Al ratio of 75 (i.e., CoZ-75-39, -78, and -143) were prepared similar to those with Si/Al = 25, except using 6 g of H-ZSM-5 (Zeolyst International; Si/Al = 75, $S_{\mathrm{BET}} = 400\ \mathrm{m^2/g}$, pore volume = 0.2 mL/g).

2.2. Catalyst characterization

2.2.1. Inductively coupled plasma atomic emission spectroscopy

The elemental composition of the synthesized catalysts was determined by inductively coupled plasma atomic emission spectroscopy (ICP-AES). Samples were initially dissolved in lithium tetraborate and heated to 1100 °C, followed by dissolution of the obtained solid in a $H_2SO_4/HNO_3/HF$ solution. The solution was then subjected to a temperature of 8000 °C obtained using a plasma torch, and the elemental composition was determined by applying Beer–Lamberts law for excitation.

2.2.2. X-Ray diffraction

X-Ray diffraction (XRD) patterns were obtained using a PHILIPS PW1050/81 goniometer with Cu-K_α radiation (λ = 1.54186 Å). Scans were recorded continuously for 2θ values ranging from 3° to 80°, with a step width of 0.02° and a dwell time of 5 s. The assignment of the crystalline structure was performed using data from the ICDD-PDF Pearson's Handbook.

2.2.3. X-Ray photoelectron spectroscopy

Samples of CoZ-25-39, -115, and -248 were each separately placed onto a sample holder and degassed in a UHV chamber with a base pressure of 1×10^{-9} Torr. The sample (typically 50 mg) was then exposed to radiation from an Al-K_α source (1486.6 eV) equipped with a monochromator, and emitted electrons were collected and analyzed by a ESCALAB 200R (Fisons Instruments) analyzer. The apparatus was calibrated with respect to the Au $4f_{7/2}$ peak. In the event of a charge effect, an internal reference, such as C_{1s} (BE = 284.6 eV), was used. The composition of the samples was determined by quantitative analysis using the cross-sections given by Scofield [17].

2.2.4. UV–vis reflectance spectroscopy

Samples of CoZ-25-39, -60, -104, -112, and -248 were studied with a Perkin–Elmer Lambda 9 spectrometer, and spectra in the 190–900 nm range were collected at ambient temperature. In addition, spectra of CoZ-25-58 pretreated by drying in air at 120 °C followed by exposure to air, drying in air at 200 °C followed by nonexposure to air, drying in air at 200 °C followed by exposure to air, and calcination at 550 °C followed by exposure to air were also collected.

2.2.5. Transmission electron microscopy

Samples (50 mg) of CoZ-25-39 and CoZ-25-248 were separately crushed and suspended in ethanol. One drop of this suspension was deposited on a copper grid covered with a carbon film. The grid was then placed in a JEOL JEM 2010 microscope, equipped with an EDX Pentaafet Link-Isis, and images were obtained at an acceleration voltage of 200 kV with a maximum resolution of 0.19 nm.

2.3. Catalytic reduction of NO

The reaction apparatus consisted of a gas feed system, the reactor section, and the analysis section. The reactant gas concentration was NO = 1000 ppm, CH_4 = 2500 ppm, H_2O = 0 or 5%, and O_2 = 5% diluted into He. For evaluating the effects of WATER and SO_2, 5% and 350 ppm were added to the feed. Then 0.5 g of the zeolite catalyst, sieved to a particle fraction of 200–300 μm, was loaded into a U-shaped Pyrex reactor and supported with glass wool. A condenser was placed immediately downstream of the reactor to trap water vapor present in the reactor effluent. A quadrupole mass spectrometer (MS) (Pegasus, VG) and an infrared (IR) cell placed in a Fourier transform infrared (Nicolet 550) spectrometer placed downstream of the condenser monitored the concentration of the reactor effluent. The IR cell allowed monitoring of NO, NO_2, N_2O, CO, and CO_2 at specific time intervals, whereas He ($m/e = 4$),

Table 1
Composition of Co-ZSM-5 catalysts as obtained from elemental ICP-AES analysis

Catalyst	Si/Al[a]	Co (wt%)	Co/Al[a]	DE[b] (%)
CoZ-25-39	25	0.71	0.19	39
CoZ-25-58	25	1.08	0.29	58
CoZ-25-104	25	1.87	0.52	104
CoZ-25-115[c]	25	2.12	0.57	115
CoZ-25-248	25	4.31	1.24	248
CoZ-75-39	75	0.24	0.19	39
CoZ-75-78	75	0.48	0.39	78
CoZ-75-143	75	0.88	0.71	143

[a] Molar ratio.
[a] DE (degree of exchange) = 200 × (Co/Al).
[a] The ion-exchange process was repeated twice for this sample.

CH_4 ($m/e = 15$), N_2 or CO ($m/e = 28$), NO ($m/e = 30$), O_2 ($m/e = 32$), CO_2 or N_2O ($m/e = 44$), and NO_2 ($m/e = 46$) were monitored continuously by the MS. Ion current profiles of each gas were converted to the respective concentration profiles with the aid of calibration factors obtained from in-house calibration. The NO reduction reaction was carried out at 25–550 °C at atmospheric pressure and at gas hourly space velocity of 8000–16,000 h^{-1}, even though significant conversion was observed only in the temperature range of 200–550 °C. The Co-ZSM-5 catalysts were pretreated before each reaction as follows: heating from 25 to 130 °C at 10 °C/min and holding at 135 °C for 15 min, followed by heating to 550 °C at 10 °C/min and holding at 550 °C for 8 h, followed by cooling to 25 °C at 20 °C/min in He.

3. Results

3.1. Elemental composition

The ion-exchange process resulted in underexchanged samples, CoZ-25-39, CoZ-25-58, CoZ-75-39, and CoZ-75-78; completely exchanged samples, CoZ-25-104 and CoZ-25-115; and overexchanged samples, CoZ-25-248 and CoZ-75-143. These are listed in Table 1.

3.2. X-Ray diffraction

The ion-exchange process clearly preserved the ZSM-5 structure, as indicated by the presence of XRD reflexes corresponding to ZSM-5 (not shown). The absence of reflexes corresponding to crystalline oxide phases of Co, CoO, or Co_3O_4 confirm that Co is present either in the exchanged position of the zeolite or in the shape of Co aggregates <30 Å in size.

3.3. X-Ray photoelectron spectroscopy

The Co 2p photoemission spectra of CoZ-25-39, CoZ-25-115, and CoZ-25-248 are shown in Fig. 1A. The Co $2p_{3/2}$ peaks for CoZ-25-39 and CoZ-25-115 appearing at 782.5 and 782.2 ± 0.2 eV, respectively, are characteristic of Co^{2+} species present at ion-exchanged positions of the zeolite [18], indicating the presence of Co not only in Co^{2+} form, but also

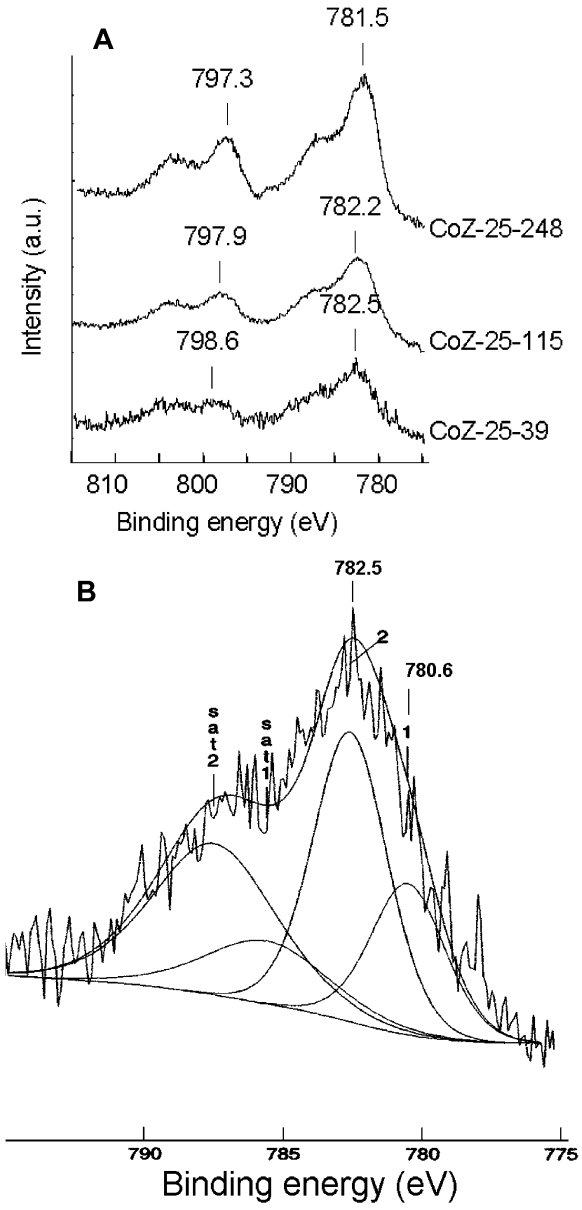

Fig. 1. (A) Co 2p photoemission spectra of CoZ-25-39, CoZ-25-115, and CoZ-25-248. (B) Peak fitting analysis of Co 2p signal for sample CoZ-25-248. Peaks 1 and 2 with their corresponding satellites sat1 and sat2 are assigned to oxide particles and Co^{2+} ions respectively.

positioned at ion-exchange sites in close interaction with the ZSM-5 lattice. The Co $2p_{3/2}$ peak for the overexchanged sample CoZ-25-248 shifted to 781.5 eV, indicating the significant presence of another form of Co in addition to Co^{2+}, such as CoO [18–21], Co_3O_4 [19–22], or Co_2O_3 [21]. From the work of Mhamdi et al. in [26], this shift could also reflect the formation of cobalt phyllosilicate outside the zeolite, specific of overexchanged material (DE = 300%). As a matter of fact, a close X-ray photoelectron spectroscopy (XPS) spectrum has been reported previously for co-silicate Co_2SiO_4 formed by reacting cobalt acetate with silica [35].

In addition to the main Co $2p_{3/2}$ peaks, satellite peaks (spin-orbital splitting) are also revealed in the XPS spectra at 778–779 eV. The relative intensity of these compared with the main

Table 2
Relative concentrations of Co^{2+} and Co oxides as calculated from XPS spectra

Catalyst	Co^{2+} (wt%)	Co oxides/silicate (wt%)
CoZ-25-39	68	32
CoZ-25-115	61	39
CoZ-25-248	49	51

Table 3
Catalyst composition evaluated from XPS spectra of CoZ-25-39, CoZ-25-115, and CoZ-25-248

Catalyst	Co (wt%)	Si/Al (molar)	Co/Al (molar)
CoZ-25-39	1.42	21.5	0.3
CoZ-25-115	7.43	17.9	1.5
CoZ-25-248	21	18.2	5.2

$2p_{3/2}$ peak may be indicative of the various forms of Co species present in the samples studied [21].

A peak-fitting analysis performed on all spectra of all the three samples resulted in the decomposition of the $2p_{3/2}$ main peak into a Co^{2+} peak at 782.5 ± 0.1 eV and a smaller peak for the various oxides/silicate adspecies at 780.6 ± 0.1 eV, as well as the decomposition of the satellite peak (spin-orbital splitting) into two peaks, as shown in Fig. 1B for CoZ-25-248. Note that all decomposition were carried out using the same parameters (binding energy, width-to-height ratio, Gaussian/Lorenzian ratio). The results of these decompositions (main peaks + satellite surfaces) are reported in Table 2. Accurate assignment of the oxide peaks (around 780.6 eV) to CoO, Co_3O_4, or Co_2O_3 was not possible, because the peak maxima obtained in the present study do not correlate exactly with those reported in the literature for pure oxides. This indicates the much likely formation of a mixture of oxide species together with silicate-like species for the overexchanged sample, as suggested above. From the quantitative evaluation of the relative amounts of Co^{2+} and Co oxides and/or silicate, considering both the $2p_{3/2}$ peaks and their satellites (Table 2), it seems that even on underexchanged catalysts, a significant presence of Co oxides is detected on or near the surface of the zeolite grains, the relative concentration of which increases progressively with increasing degree of exchange. The relative concentration of these outside adspecies (possibly including cobalt silicate) tend to be as important (or even more important) as the internal Co^{2+} species on CoZ-25-248.

Table 3 gives the elemental composition of the three catalysts evaluated from their respective XPS spectra. The Si/Al ratios of all three catalysts obtained from the XPS spectra are lower than those values obtained from ICP analysis (Table 1), indicating enrichment of the surface with Al possibly occurring during the ion-exchange/calcination process. The Al surface enrichment could also point to a partial dealumination process not detectable by XRD. Another explanation (especially for the overexchanged samples) could be the formation of Co silicates outside the zeolite, as suggested above, thereby decreasing the concentration of Si at the zeolite surface. Table 3 also shows higher values for Co content than those estimated by ICP analysis, indicating the preferential formation of extra-framework Co particles. The deconvolution of the XPS spectra (Fig. 1B) and the subsequent quantitative evaluation of the Co/Al ratio also indicate a preferential formation of extra-framework particles, as discussed earlier in this section.

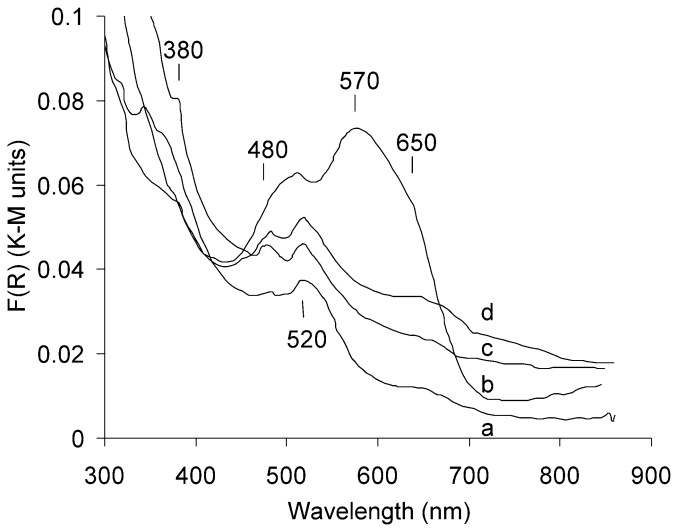

Fig. 2. UV–vis spectra of as-synthesised CoZ-25-58: (a) dried at 120 °C in air followed by exposure to air, (b) dried at 200 °C in air without further exposure to air, (c) dried at 200 °C then exposed to air, and (d) calcined in He at 550 °C followed by exposure to air.

3.4. UV–vis spectroscopy

Fig. 2 presents the UV–vis spectra collected for the as-synthesised CoZ-25-58 after various treatments. Spectra of samples exposed to air during data collection may represent Co species that may have supplemented their coordination spheres on account of air exposure. The spectrum of CoZ-25-58 exposed to air after drying the as-synthesized sample in air at 120 °C (Fig. 2, curve a), exhibits shoulder peaks at 345, 380, and 650 nm, as well as peaks at 480 and 520 nm. The presence of Co_3O_4, evidenced by the appearance of shoulder peaks at 345, 380, and 650 nm (Table 4), would result from the drying process at 120 °C, during which Co hydroxyls, formed during the wet ion-exchange process, are sequentially oxidized to this form of Co oxide. The observation of the peak at 480 nm, assigned to Co^{2+} species coordinated octahedrally [23], provides further evidence of the sequential oxidation process for this case up to CoO. The peak at 520 nm does not match any of the Co peaks reported in the literature, as summarized in Table 4; however, the possibility that the 520-nm peak represents the Co^{2+} species coordinated octahedrally as either $[Co(H_2O)_6]^{2+}$ or $[Co(H_2O)_5OH]^{+}$, reported at 500 nm, cannot be ruled out. Drying CoZ-25-58 at 200 °C (Fig. 2, curve c) or calcining in He at 550 °C (Fig. 2, curve d) with further exposure to air produced no significant changes in the 380-, 480-, 520-, and 650-nm peaks. In summary, CoZ-25-58, even after calcination in He at 550 °C and subsequent exposure to air, contained Co in Co_3O_4, CoO, and $[Co(H_2O)_6]^{2+}$ or $[Co(H_2O)_5OH]^{+}$ form.

The spectrum collected in the absence of air after drying the as-synthesized CoZ-25-58 in air at 200 °C (Fig. 2, curve b) differs significantly from the other spectra described above. The

Table 4
Reported assignment of UV–vis peaks for various Co species

Sample	Wavenumber (cm^{-1})	Assignment	Reference
Co/Al_2O_3	380 670	Co_3O_4	[23]
CoNa-ZSM-5	455 498	Co^{2+} ions in the sinusoidal channel of ZSM-5 (γ sites)	[11]
Co/Al_2O_3	480	Octahedrally coordinated Co^{2+} ions	[23]
Co-ZSM-5	440–560 (broad)	Octahedrally coordinated Co^{2+} ions	[23]
Co-ZSM-5	500	Co^{2+} in octahedral symmetry as either $[Co(H_2O)_6]^{2+}$ or $[Co(H_2O)_5OH]^{+}$	[22]
CoNa-ZSM-5	472 538 583 625	Co^{2+} ions located close to the plane of the six-membered ring (β site)	[11]
CoNa-ZSM-5	662	Co^{2+} ions coordinated to the rectangle of four O atoms of the walls of the main ZSM-5 channels (α site)	[11]

two peaks at 500 and 590 nm and the shoulder at 640 nm are comparable to the spectra of CoNa-ZSM-5 reported earlier [11], and, as reported earlier, these peaks could be deconvoluted into a triplet represented by the 538-, 583-, and 625-nm peaks and a doublet comprising the 455- and 498-nm peaks. The triplet is representative of Co^{2+} ions present in the vicinity of a six-member ring at the intersection of straight and sinusoidal channels in the ZSM-5 structure and denoted as β sites; the doublet is representative of Co^{2+} ions located in the sinusoidal channel of the ZSM-5 structure and denoted as γ sites [11]. For the dried CoZ-25-58, prevention of exposure to air appears to favor the exchange of Co ions at β and γ sites over the Co oxides, CoO and Co_3O_4.

Fig. 3 shows the spectra of calcined underexchanged, completely exchanged, and overexchanged CoZ-25 samples collected in the presence of air. The underexchanged samples, CoZ-25-40 and CoZ-25-58 (Fig. 2, curves a and b) exhibit peaks at 380 and 650 nm and at 480 and 520 nm, indicating the presence of Co_3O_4, CoO, and $[Co(H_2O)_6]^{2+}$ or $[Co(H_2O)_5OH]^{+}$ species, respectively. The completely exchanged samples, CoZ-25-104 and CoZ-25-112, (Fig. 2, curves c and d) exhibit broad peaks at 500, 590, and 640 nm, similar to those exhibited by dried CoZ-25-58 in the absence of air (Fig. 2, curve b), indicating the presence of Co at the β and γ sites. The overexchanged sample, CoZ-25-248 (Fig. 2, curve e) exhibits the same peaks as the completely exchanged samples, but with a higher relative intensity of the 640-nm peak. This could be assigned to Co ions present at α sites after deconvolution [11].

To summarize, the significant increase in the intensity of the UV–vis bands at 300–700 nm with the degree of exchange clearly reveals (i) the increasing concentration of external Co oxides (Co_3O_4 at 380 and 640 nm and CoO at 480 nm) and

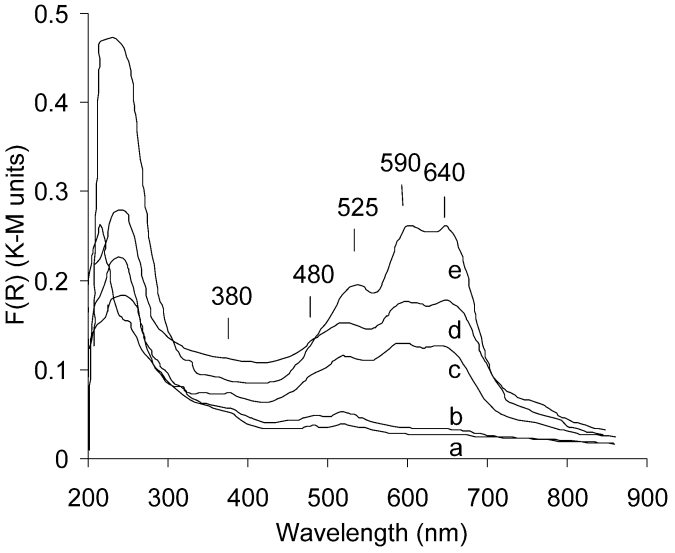

Fig. 3. Influence of the Co exchange degree of calcined CoZ-25 samples on the UV–vis spectra registered in air at room temperature: (a) CoZ-25-39, (b) CoZ-25-58, (c) CoZ-25-104, (d) CoZ-25-112, and (e) CoZ-25-248.

their relative hydroxylated species, and (ii) the relative change from an octahedral (480–520 nm) to a tetrahedral (triplet at 525, 590, and 640 nm) Co^{2+} ion configuration. In that sense, the increased concentration of Co ions in α tetrahedral positions (easily accessible and less stable) proceeds at the expense of the β octahedral positions, essentially due to the fact that the α positions are more numerous than the β ones and thus are favored at higher Co concentrations. The observation that the band at 345–380 nm is more intense for CoZ-25-112 than for the overexchanged CoZ-25-248 could tentatively come from the appearance of silicate at high Co concentrations at the expense of Co oxide particles, as suggested earlier.

3.5. Transmission electron microscopy

Fig. 4 shows transmission electron microscopy (TEM) images of a zeolite grain of CoZ-25-39 after short (Fig. 4A) and long exposures (Fig. 4A) to the high-energy beam. The stacking of 220 × 90 nm hexagonal ZSM-5 plates that appear to be well crystallized is clearly observed in Fig. 4A. The image also does not indicate the presence of Co in any oxide form, suggesting that most of the Co phase present in the underexchanged sample (as evidenced from XPS and UV–vis results) may be distributed inside the ZSM-5 channels. The high-resolution image of CoZ-25-39 photographed along the [100] plane of the ZSM-5 channel and the fast Fourier transform-derived image (Fig. 5) confirm the rhombohedral crystalline structure of ZSM-5. The entry to the ZSM-5 mesopores, identified by the white luminous spots characteristic of the electron density, does not seem to be blocked by cobalt oxide microparticles. EDX analysis performed at specific spots on the image confirmed the uniform distribution of Co in the zeolite grains and indicated Si/Al and Co/Al ratios of 25 and 0.21, respectively, both in agreement with the results of the ICP analysis. Therefore, according to the previous XRD, XPS, and UV–vis analyses, the uniformly distributed Co must be present at ion-exchange sites (essentially α

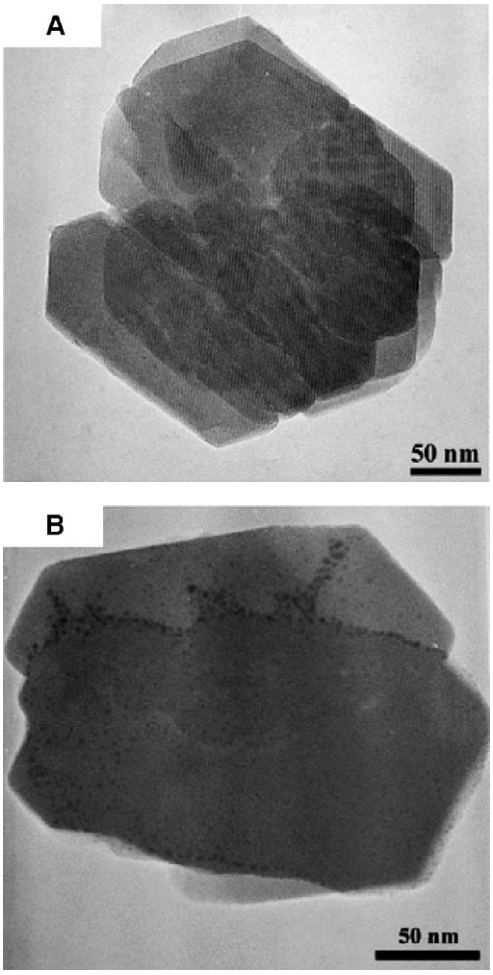

Fig. 4. TEM images of sample CoZ-25-39 after (A) short exposure and (B) long exposure to the electron beam.

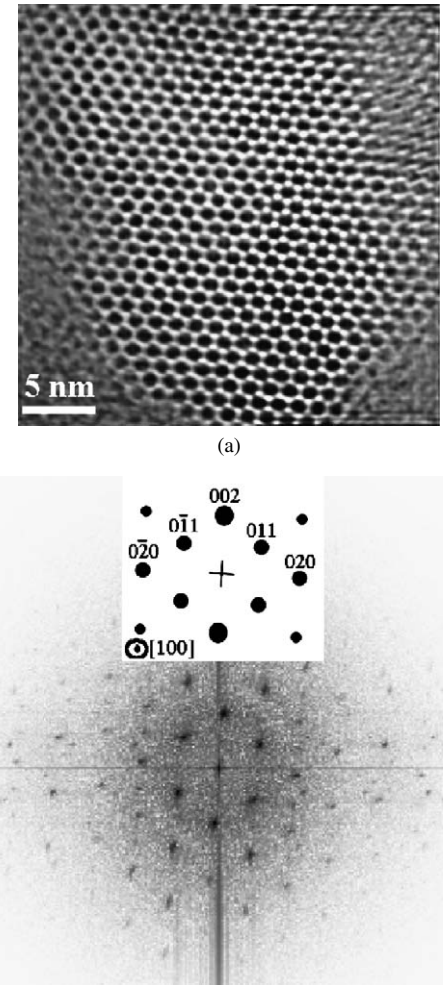

Fig. 5. HR-TEM image along the [100] plane of sample CoZ-25-39 and the corresponding fast Fourier transform derived image.

and β) and also may be present in the shape of microaggregates <6 Å in size.

Prolonged exposure to the high-energy beam appears to destroy the ZSM-5 channels, as shown in the images of superimposed ZSM-5 plates in Fig. 4B. The destruction of the ZSM-5 lattice seems to have caused sintering and rapid migration of the Co ions/aggregates to the zeolite grain periphery. The regular distribution of the sintered Co particles at the periphery and their uniform size of 2 nm confirm the uniform distribution of Co in the ZSM-5 channels before sintering.

Fig. 6 shows TEM images of the overexchanged CoZ-25-248 collected after both short- and long-term electron beam exposures. The photograph of a first single ZSM-5 plate 240 × 160 nm in size (Fig. 6A) clearly shows a crystalline structure with no observable Co oxides. EDX analysis revealed an Si/Al ratio of 25, in agreement with that obtained from ICP analysis, whereas the Co/Al ratio of 0.7 was significantly lower than that of 1.24 obtained from ICP analysis. The Co/Al value indicates that Co ions present at the ion-exchange sites correspond to a 140% exchange, with the remainder of the Co present as aggregates. The presence of large (20 nm) Co oxide particles is clearly shown in the image obtained on another ZSM-5 grain after both short- and long-term exposure (Fig. 6B). Smaller particles (2–5 nm) are also observed after prolonged exposure; these could result from the sintering of Co particles due to the high-energy beam. Another structure of cobalt oxide species in the form of "wires" or "plates" is observed with another ZSM-5 grain (Fig. 6C). This tends to confirm the previous hypothesis that for the overexchanged sample, silicate-like deposits would form around the zeolite grains, in accordance with previous reports [26].

3.6. Catalytic performance for selective NO reduction

Fig. 7 shows the conversion of NO and CH_4 as well as the selectivity to N_2 and NO_2 exhibited by CoZ-25-104 during the NO reduction reaction from 200 to 550 °C. CoZ-25-104 starts to exhibit appreciable NO conversion activity at 290 °C, which gradually increases to a maximum of 60% at 500 °C. Further increase in temperature to 550 °C leads to a decrease in NO conversion. N_2 selectivity and CH_4 conversion also increase with increasing temperature; N_2 selectivity reaches a maximum and remaining stable at 500 °C, whereas CH_4, activated at 375 °C, is completely oxidized at 550 °C. The absence of N_2O and the presence of NO_2 in the product stream suggest the occurrence

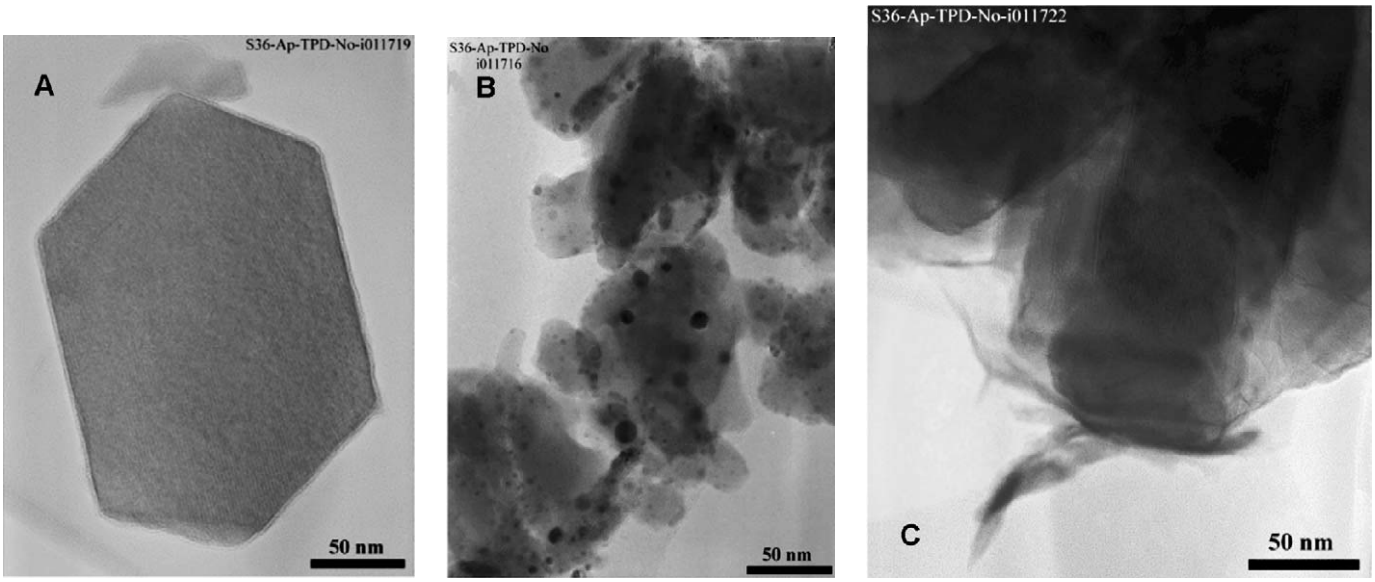

Fig. 6. TEM images of sample CoZ-25-248 after (A) short exposure, (B) long exposure to the electron beam, and (C) cobalt oxide wires.

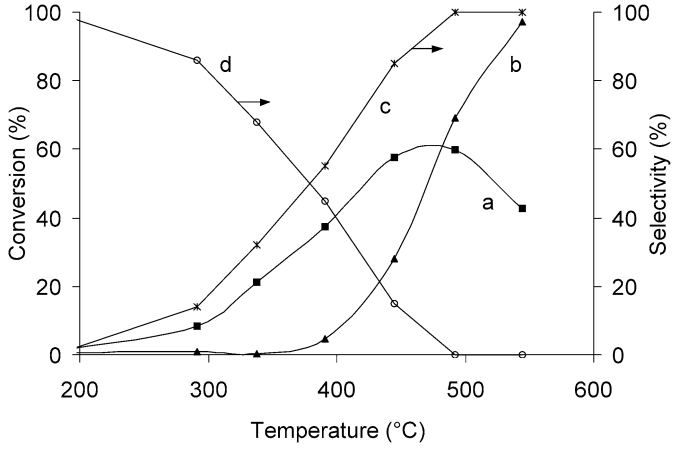

Fig. 7. Catalytic performance of sample CoZ-25-104 as a function of temperature: (a) NO conversion, (b) CH_4 conversion, (c) selectivity to N_2, and (d) selectivity to NO_2. Reaction conditions: [NO] = 1000 ppm, [CH_4] = 2500 ppm, and [O_2] = 5%.

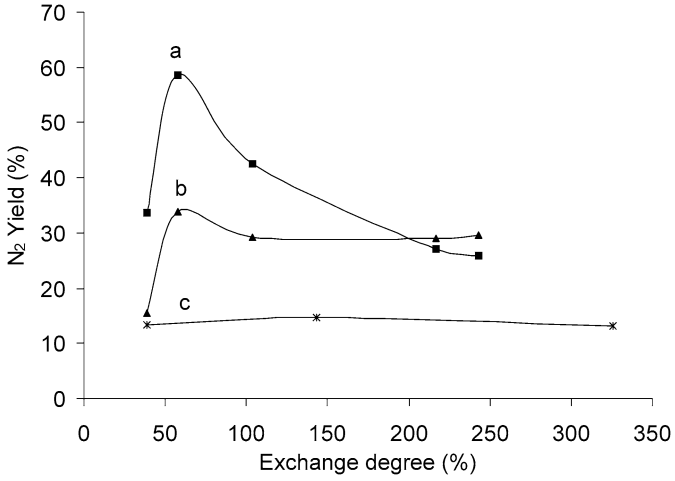

Fig. 8. Influence of the exchange degree of CoZ-25 and CoZ-75 samples on the N_2 yield. CoZ-25, [NO] = 1000 ppm, [CH_4] = 2500 ppm, [O_2] = 5%: (a) 0% H_2O, (b) 5% H_2O, (c) CoZ-75 (reaction conditions identical to b); T = 550 °C.

of NO oxidation reaction, which, although significant at temperatures below 400 °C declines to a negligible value at 500 °C.

3.6.1. *Effect of Co content*

Fig. 8 (curve a) reports the changes in N_2 yield as a function of the degree of exchange obtained at 550 °C for a VHSV of 15,000 h^{-1}. As shown, the best N_2 yields are obtained for the underexchanged CoZ-25-58 among all of the catalysts tested. Note that these values compare well with data reported previously, although slightly different operating conditions preclude a strict data comparison [24,25].

An increase in the degree of Co exchange from 58 to 243% led to decreases in both N_2 yield and the temperature at which maximum NO conversion occurred, from 500 C to 445 °C. CH_4 conversion (not reported here) increased with temperature for all catalysts and reached 100% at 550 °C for the completely exchanged and overexchanged catalysts. In addition, the CH_4 light-off temperature is more than 100 °C lower for the overexchanged CoZ-25-243 than for the underexchanged CoZ-25-39. To summarize, these results clearly show that (i) overexchanged Co-ZSM-5 catalysts favor CH_4 combustion compared with the NO reduction reaction, (ii) active sites promoting NO to NO_2 oxidation and CH_4 oxidation at low temperatures are present on the overexchanged catalysts, and (iii) the active sites facilitating NO reduction with high N_2 selectivity at high temperatures are essentially dominant in underexchanged catalysts.

The TOF values for the NO reduction based on the total cobalt content for the underexchanged, completely exchanged, and overexchanged CoZ-25 catalysts were calculated at 200–550 °C, as shown in Fig. 9. An initial observation is that the highest values of TOF per cobalt atom, observed for the underexchanged samples CoZ-25-39 and CoZ-25-58, were close to 2.5×10^{-4} s^{-1}, comparable to those reported previously [24,25] even though, as stressed earlier, the operating condi-

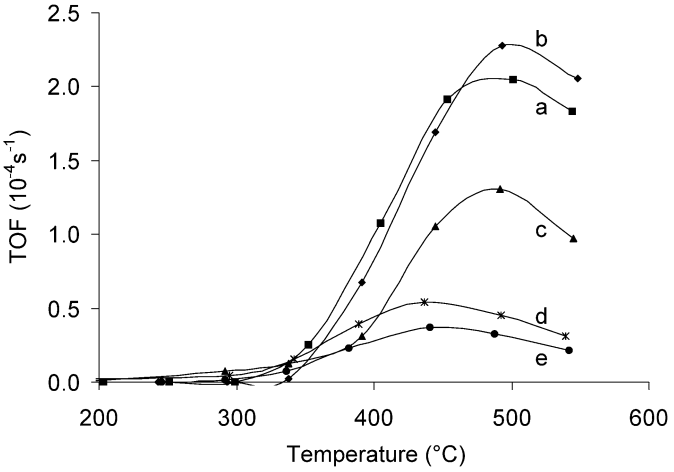

Fig. 9. TOF values as a function of temperature for CoZ-25 samples: (a) CoZ-25-39, (b) CoZ-25-58, (c) CoZ-25-104, (d) CoZ-25-217, and (e) CoZ-25-248.

tions (e.g., the NO/CH_4 ratio) are slightly different. A second observation is that the TOF values clearly vary with the degree of exchange, indicating that not all cobalt atoms are uniformly active for the NO reduction. Thus the TOF values for the underexchanged CoZ-25-39 (Fig. 9a) and -58 (Fig. 9b) do not change significantly, while those for the completely exchanged CoZ-25-104 (Fig. 9c) decrease significantly and those for the overexchanged CoZ-25-217 (Fig. 9d) and -248 (Fig. 9e) tend to stabilize at low values. Thus the general trend (discussed in detail later) is that at low Co content, all of the cobalt atoms are active and selective with the same intrinsic activity; at intermediate content, much less active or inactive Co species must be considered in addition to the previous ones; and at high Co content, a prominent fraction of the Co atoms is no only a little more active and selective.

3.6.2. *Effect of Si/Al ratio*

The Si/Al ratio of the ZSM-5 zeolite directly determines the number of exchangeable sites and thus the potential for acidity. The acidity of the catalyst will be high if the Si/Al ratio is low and if the exchange of protons by cobalt cations is not complete. The present study compares two Co-ZSM-5 catalysts (CoZ-25-39 and CoZ-75-39) with different Si/Al ratios (25 and 75) but with the same degree of Co exchange (39%). Fig. 10 shows NO and CH_4 conversions, as well as N_2 selectivity, as a function of temperature during NO reduction in the presence of CH_4 and in the excess of O_2 at 200–550 °C. CoZ-75-39 exhibits higher NO conversion than CoZ-25-39 below 400 °C, but CoZ-25-39 shows a maximum NO conversion of 38% at 500 °C, whereas CoZ-75-39 nearly stabilizes at 28% at 400–500 °C. But the N_2 selectivity for CoZ-75-39 is lower than that for CoZ-25-39 at all temperatures between 200 and 550 °C. The higher NO conversion and lower N_2 selectivity for CoZ-75-39 below 400 °C indicate the oxidation of NO to NO_2 at the expense of N_2 formation. The increased NO oxidation on CoZ-75-39 correlates well with the expected presence of Co in the form of an outer Co_3O_4 phase in a catalyst with a high Si/Al ratio, and thus a low concentration of exchangeable sites for inner Co species. As shown in Fig. 10A, the higher Si/Al ratio does not appear to influence CH_4 conversion, which could indicate either diffusional limitations or the presence of Co_3O_4 in very low quantities on Co-Z-75-39.

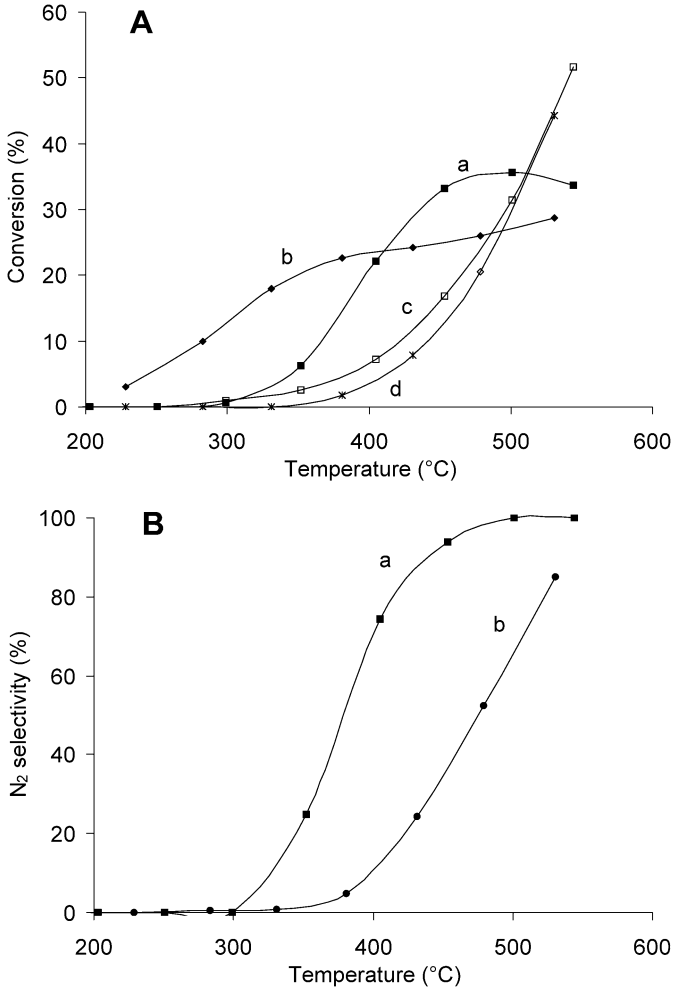

Fig. 10. Influence of the Si/Al ratio (A) on the conversion of NO: (a) CoZ-25-39; and (b) CoZ-75-39; and on the conversion of CH_4: (c) CoZ-25-39 and (d) CoZ-75-39; and (B) on the selectivity to N_2: (a) CoZ-25-39 and (b) CoZ-75-39, as a function of temperature. Reaction conditions: [NO] = 1000 ppm, $[CH_4] = 2500$ ppm, and $[O_2] = 5\%$.

3.6.3. *Effect of water*

Fig. 8 (curve b) describes the effect of adding 5% water to the feed on N_2 yield as a function of the degree of exchange at 550 °C, that is, under conditions at which the best performance is observed. Adding water led to a decrease in the maximum N_2 yield by about 50% on the underexchanged CoZ-25-39 and CoZ-25-58, a 37% decrease on the completely exchanged CoZ-25-104, and practically no change on the overexchanged CoZ-25-217 and CoZ-25-248 samples. Note that for all catalysts, essentially the activity, and not the N_2 selectivity, was affected by the addition of water.

As shown in Fig. 8 (curve c), at a higher Si/Al ratio in the Co-ZSM-5 catalysts (75 compared with 25), adding water led to a further decrease in performance. Therefore, the detrimental effect of water on NO reduction activity is probably not linked to a decrease of active sites via dealumination, because in that

case better resistance of the catalysts exhibiting a higher Si/Al ratio would be expected. A much more likely effect of water, as discussed later, is to poison the active sites by preferential adsorption and/or to induce a sintering effect by leaching the active sites out of the zeolite structure. As a matter of fact, these active sites can conceivably be located at the acid sites, the concentration of which depends on the Si/Al ratio and the degree of exchange. The increase in the activation temperature of CH_4 in the presence of water also suggests that water competitively adsorbs on the sites responsible for CH_4 activation.

Long-term stability tests were carried out on the underexchanged CoZ-25-39 and CoZ-25-58 samples in the presence of water. An initial decrease in N_2 selectivity (by about 20%), followed by its stabilization with longer operation, can be attributed to the partial irreversible destruction of the acid sites located at the edges of the internal active sites and/or to the progressive leaching of the Co aggregates in the presence of water. Some experiments carried out in the presence of higher water pressure (ca. 10%) revealed the same trends in catalyst deactivation, suggesting that the kinetic of catalyst aging (probably linked to cobalt-phase restructuring) is slightly dependent on vapor pressure.

3.6.4. Effect of SO_2

Fig. 11 shows the changes in NO and CH_4 conversions observed for CoZ-25-39 after the introduction of 350 ppm of SO_2 during NO reduction in the presence of CH_4 and excess O_2 at 550 °C. Adding SO_2 led to a 35% decrease in NO conversion (i.e., from 28 to 18%) and a 60% decrease in CH_4 conversion in the first hour. CoZ-25-39 subsequently exhibited stable NO and CH_4 conversions for up to 5 h. The significant initial decline in CH_4 conversion combined with a less severe decrease in NO conversion meant that the selectivity of the reaction to NO reduction was enhanced by the presence of SO_2. The inhibition of CH_4 total oxidation by O_2 and the less severe decline in NO reduction are probably related to the preferential deposition of SO_2 on the sites active for the combustion reaction, that is, Co oxides present on the zeolite outer surface. Removing SO_2 from the reaction stream led to only partial recovery of both NO and CH_4 conversion, suggesting an irreversible poisoning of some active sites by SO_2. Similar effects were observed on the other underexchanged catalyst, CoZ-25-58.

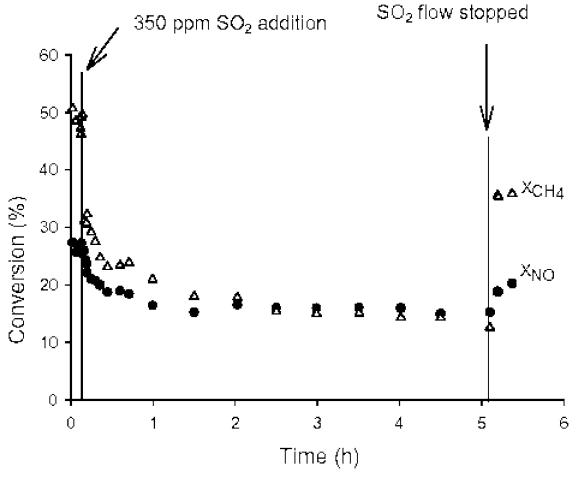

Fig. 11. Performance of CoZ-25-39 with time on stream containing SO_2. Reaction conditions: [NO] = 880 ppm, [CH_4] = 3000 ppm, [O_2] = 5%, [SO_2] = 350 ppm, GHSV = 8000 h^{-1}, T = 550 °C.

3.7. Postreaction characterization

XRD patterns of the underexchanged, completely exchanged, and overexchanged CoZ-25 and CoZ-75 subjected to NO reduction in the absence and presence of water did not indicate the presence of Co_3O_4 or CoO. UV–vis spectra of all catalysts regardless of Si/Al ratio and degree of exchange after operation in NO reduction were similar to those obtained before reaction. But after being subjected to NO reduction in the presence of water, the catalysts displayed different UV–vis spectra (not shown) compared with the prereaction catalysts. The intensity of the peaks representing Co_3O_4 and CoO species present in an octahedral configuration was increased in the postreaction catalysts, with a stronger relative increase for completely exchanged and overexchanged catalysts. The presence of water in an oxidizing atmosphere possibly promotes migration of the Co^{2+} species from the positions of exchange to the exterior and formation of CoO species, whereas the increase in Co_3O_4 could be the result of particle agglomeration in the presence of water.

4. Discussion

4.1. Inventory of cobalt species in the reacting systems

Characterization of the Co-ZSM-5 catalysts before and after the NO reduction reaction provides insight into the specific actions of the various cobalt species. Three different species are postulated in all investigated samples: (i) cations located at ion-exchanged position, (ii) microaggregates inside the zeolite framework, and (iii) cobalt oxides/silicates outside the zeolite framework. Their relative amounts are determined by Co loading, degree of exchange, Si/Al ratio, and experimental conditions.

4.1.1. Cations located at ion-exchanged position

Investigations using UV–vis spectroscopy revealed the presence of both Co^{2+} cations in a tetrahedral environment located at α sites (along the wall of the channels) and octahedral Co^{2+} located at β sites (at the intersection of channels). Fig. 12 illustrates the change in geometry of the cations during the various stages of catalyst pretreatment. In solution, cobalt cations form octahedral complexes with water of type $Co(H_2O)_6{}^{2+}$ or $Co(H_2O)_5(OH)^+$. These cations are involved in the ion-exchange process. The calcination step allows the release of the water molecules from the complexes and the embedment of Co^{2+} cations in the tetrahedral α position of the zeolite. Exposure of the zeolite to air at room temperature led to rehydration of the cations, with the subsequent formation of pseudo-octahedral complexes. A rise in temperature during calcination pretreatment induced a shift of the cations from α sites to octahedral β sites. The recovery of the cations in the initial position

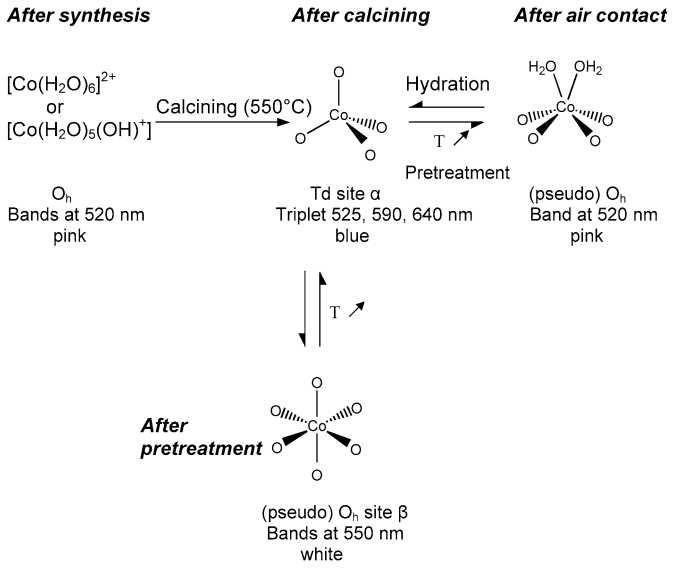

Fig. 12. Schematic changes in the state of Co during various stages of catalyst pre-treatments.

α after reexposure of the zeolite to air (Fig. 2, curve c) demonstrates the reversibility of the shift from the α position to the β position.

The location of the Co^{2+} cations in α or β sites depends on the degree of exchange. When the DE value is >60%, cations are preferentially located in tetrahedral sites, because the number of α sites on the wall of the channels is larger than the number of β sites at the intersection of channels. Most of the cations remain in tetrahedral positions, but a small part of Co^{2+} is hydrated and shifts to β sites [22]. In contrast, at low degrees of exchange (<60%), tetrahedral cations in α sites might migrate to β positions depending on the temperature. The octahedral sites become the predominant location for cobalt cations at high temperatures [27], with cobalt atoms having a large number of atoms in their coordination spheres. Electron-donating molecules like H_2O or NO will less readily coordinate to the cations in β sites. The cobalt in β sites is thus more passive toward the molecules involved in the reaction. In contrast, Co^{2+} cations located in the α position will react with NO to form dinitrosyl species, reported as potential intermediate species in the decomposition of NO on Cu-ZSM-5 [27–29].

4.1.2. Microaggregates

In addition to the isolated cobalt cations, partial clustering of cobalt ions within the zeolite framework is postulated. As a matter of fact, EXAFS studies carried out on close systems [30,31] have indicated the formation of microaggregates containing up to 15 atoms, which could mean a maximum of about 7 Co atoms per cluster, assuming a CoO-like structure. Their formation can be explained by the clustering of a limited number of tetrahedral cobalt cations originating from α positions, with extra-framework oxygen atoms and/or OH groups to complete the coordination sphere, acting in the building of microaggregates [31]. Because the mean value of the channel opening in ZSM-5 is 5.5 Å, these microaggregates are most likely located inside the zeolite cage (diameter of about 8–9 Å) at the intersection of the channels, minimizing any interference with the diffusion of reactants and products. Microaggregates smaller than 8–9 Å cannot be detected by XRD or TEM, resulting in a poorly documented structure. Only water could speed up this process by hydrating the cations, for example, during the synthesis. Coordinated water could lead to progressive leaching of the isolated cobalt cations, which would agglomerate and precipitate to form microaggregates.

4.1.3. Cobalt oxides and silicates

Cobalt oxides (i.e., CoO and Co_3O_4) are the third category of species observed on the prepared Co-ZSM-5. Their formation might occur during the drying or the calcination step and could involve hydroxide species according to the following scheme [32]:

$$Co(H_2O)_4(OH)_2 \overset{60\,^\circ C}{\rightarrow} Co(OH)_2 \overset{100\,^\circ C,\mathrm{air}}{\rightarrow} CoO \overset{100\,^\circ C,\mathrm{air}}{\rightarrow} Co_3O_4.$$

Another route for the formation of cobalt oxides is in direct relation to the proposed mechanism for microaggregate formation. In the presence of water, hydrated microaggregates could migrate at the outer surface of zeolite grains. Their agglomeration would lead to particles of substantial size with crystalline structures identified as CoO and Co_3O_4. The XPS analysis shows a linear enrichment in cobalt oxides of the surface as a function of cobalt loading when the degree of exchange is >40%. High DE values are achieved by increasing the concentration of cobalt ions species in solution, leading to a high concentration of hydroxides in solution. The probable precipitation of the hydroxide species results in the formation of oxides on thermal treatment. Moreover, the distance between isolated cations at exchange sites decreases with increasing DE values. Low distances should promote their clustering. As a result, overexchanged samples have high quantities of cobalt oxides, mainly Co_3O_4. However, for this specific case, part of these cobalt oxides (or hydroxides) could react with the zeolite surface to form silicate deposits (essentially as layered structures), as observed in this work and also reported elsewhere [26]. In the case of underexchanged samples, cobalt oxides form, but to a lesser extent (only 32 wt% of cobalt oxides for the CoZ-25-39 sample, as shown in Table 2). However, the UV–vis and XPS studies indicate that among the Co oxides, CoO is predominant at DE values <40%. CoO particles could form primarily at defect sites of the zeolite. The migration of the primary CoO particles at the outer surface of the zeolite, followed by a sintering process, would result in the formation of Co_3O_4 particles.

4.2. Specificities of the identified cobalt species in the deNO$_x$ process

The present work also has addressed the relationship between active sites of Co-ZSM-5 and activity in the reduction of NO by CH_4 in the presence of oxygen. First, overexchanged samples show catalytic activity but high selectively to NO_2. at low temperatures. At higher temperatures, the deNO$_x$ reaction almost does not occur, and methane is mainly fully oxidized to carbon dioxide. In these materials, that preferential oxidation of NO and CH_4 likely occurs essentially on the outer ox-

ide/silicate deposits, which are the main and first sites available to reactants [14]. As such, overexchanged Co-ZSM-5 can be considered poor deNO_x catalysts. Conversely, the selective reduction of NO must proceed internally.

The reduction of NO by CH_4 in the presence of O_2 involves two molecules of NO, one molecule of CH_4, and one molecule of O_2 [reaction (1)], and at least several elementary steps are generally considered concerted [13,16]. From this, it can be inferred that reaction of all of these molecules on isolated sites is highly unlikely [33]. Therefore, isolated Co cations cannot be considered active sites; they can play only an indirect role in the deNO_x process, allowing chemisorption of NO molecules into mononitrosyl and dinitrosyl cobalt species, as reported elsewhere [12,13]. In this respect, they would act as storage sites for the NO molecules to be reduced elsewhere on the proper active deNO_x sites.

From the above analysis, it can be inferred that the directly active and selective sites for the reduction of NO on Co-ZSM-5 are the microaggregates of cobalt located in the pores or the grain joints of ZSM-5. In that sense, the observation that the TOF values obtained at exchange degree <60% (Figs. 9a and b) depend little on the Co content indicates that at low cobalt concentrations, cobalt microaggregates are the main Co species present in the zeolitic system and display a constant intrinsic activity. In contrast, a significant decrease in TOF values is observed at an exchange degree >60% at intermediate Co content (Fig. 9c). Such a decrease can hardly be assigned to decreased cobalt dispersion in the microaggregates. As a matter of fact, even if some increase in the size of the cobalt microaggregates could occur at higher Co concentration, their maximum size (below about 8–9 Å) guarantees complete access of all of the Co atoms to the reacting molecules (i.e., 100% dispersion as deduced from elementary crystal modeling). A much more likely explanation is that at higher Co concentrations, not all of the cobalt atoms form microaggregates, due to limited space at channel intersections, and that in addition to isolated cobalt cations (which are not directly active, as discussed above), other inactive or less active species develop, such as the external oxide particles in which part of the cobalt is not accessible to reactants. As a matter of fact, because the TOF values are calculated on the basis of the total number of cobalt atoms, the decrease in TOF values reflects only the appearance of inactive or nonselective NO reduction sites at an exchange degree >60%.

For the highly overexchanged samples, the calculated TOF tends to stabilize at very low values (approximately one order of magnitude less than for the underexchanged material; see Figs. 9d and e). This indicates that in addition to the large amount of inactive cobalt species (large grains of cobalt oxides), any additional cobalt becomes accessible to the reactant but is very poorly active. This might fit with the development of the layered cobalt silicates in that domain of high Co content.

4.3. Stability of the active sites

Postreaction characterization gives evidence of the stability of the active sites. In the absence of water and sulfur dioxide, the UV–vis analysis reveals no modification of the catalyst composition after the deNO_x reaction. The stability of the active sites during the reaction shows that NO and CH_4 do not modify the structure of the active sites [5]. In the presence of water, a reversible effect is observed after a short exposure, but this effect becomes irreversible after prolonged exposure beyond 10 h. The reversible deactivation can be explained by the adsorption of water on the active sites [34]. This adsorption is generally reversible, leading to the recovery of the initial activity after water is removed from the stream. On the other hand, prolonged exposure to a stream containing water leads first to the reversible adsorption of water, followed by migration of the hydrated cobalt cations located in α-position and agglomeration of the microaggregates in the shape of oxide particles. The irreversible deactivation of the active sites is thus associated with the formation of CoO and Co_3O_4. Water is also known to initiate the dealumination of zeolites at high temperatures [30]. In the present case, a possible leaching of aluminum from the zeolite framework during long-term operations would modify the strength of the acid sites and thus also the reactivity of the microaggregates, because these are tightly interacting with the OH groups of the zeolite, as clearly revealed by the in situ DRIFTS analyses reported previously [13]. Water could also act on the kinetics of the parallel reactions by accelerating the desorption of NO_2 and CO_2. This kinetic effect might explain the enhancement of the catalytic activity over the overexchanged catalysts at low temperatures.

Sulfur dioxide has an effect comparable effect to that of water, with a partially irreversible deactivation of zeolite. This observation is in disagreement with results of Li and Armor [24] indicating increased catalytic activity at high temperatures induced by SO_2. The gain in activity is attributed to poisoning of the sites responsible for the direct combustion of CH_4. For the underexchanged samples (e.g., CoZ-25-39 in Fig. 11), a rapid, irreversible deactivation is observed during the first hours on stream before stable activity is achieved. TEM analysis after reaction reveals no modification of the zeolite crystallinity, formation of additional cobalt oxide species, or migration of cobalt to the outer surface of the zeolite grains. Therefore, the effect of SO_2 might be associated either with the destruction of some microaggregates promoted by a change in the interaction of the cobalt with the zeolite or with modification of the active sites. In the presence of oxygen, SO_2 may form sulfates on the active sites, as evidenced by IR spectroscopy for Fe-ZSM-5 exposed to a stream containing SO_2 [5], thus decreasing the accessibility of sites for NO and CH_4. These sulfate species could be stable under the reaction conditions to provoke the irreversible deactivation.

5. Conclusion

Detailed characterization of cobalt-exchanged ZSM-5 zeolites enabled us to distinguish the reactivity of various cobalt species observed. Amorphous microaggregates originating from Co^{2+} cations in α or β position interior of the zeolite were identified as active site for the selective reduction of NO by methane. These microaggregates grouping during the catalyst

pretreatment several cobalt and oxygen atoms, but always fully exposed to gaseous or adsorbed reacting species, are preferentially formed at low exchange degrees, whereas cobalt oxides and possibly silicates are predominant at higher exchange degrees. These latter cobalt oxides/silicates show much lower activity in selective NO reduction (reinforced by a decreasing dispersion), but favor the unselective total combustion of methane and oxidation of NO to NO_2 in the presence of oxygen. On the basis of this inventory of active species (selective and unselective), an advanced exploitation of steady-state and non-steady-state kinetics with a precise quantification of the active sites and reacting intermediates is now possible [36].

Acknowledgments

Our Colleagues from Boreskov Institute of Catalysis, L.G. Pinaeva, E.M. Sadovskaya, V.A. Sadykov and B.S. Balźhinimaev are warmly thanked for numerous and fruitful discussions on the subject.

References

[1] M. Shelef, Chem. Rev. 95 (1995) 209.
[2] G. Ramis, G. Busca, F. Bregani, P. Forzatti, Appl. Catal. 64 (1990) 259.
[3] M. Koebel, M. Elsener, M. Kleemann, Catal. Today 59 (2000) 335.
[4] Y. Li, J.N. Armor, Appl. Catal. B: Env. 1 (1992) L31.
[5] Y. Li, J.N. Armor, Appl. Catal. B: Env. 2 (1993) 239.
[6] J.N. Armor, Appl. Catal. B: Env. 1 (1992) 221.
[7] M. Iwamoto, H. Hamada, Catal. Today 10 (1991) 57.
[8] J.N. Armor, T.S. Farris, Appl. Catal. B: Env. 4 (1994) L11.
[9] X. Wang, H.-Y. Chen, W.M.H. Sachtler, Appl. Catal. B: Env. 26 (2000) L227.
[10] X. Wang, H.-Y. Chen, W.M.H. Sachtler, Appl. Catal. B: Env. 29 (2001) 47.
[11] J. Dedecek, D. Kaucky, B. Wichterlova, Microporous Mesoporous Mater. 35–36 (2000) 483.
[12] L.G. Pinaeva, E.M. Sadovskaya, A.P. Suknev, V.B. Goncharov, V.A. Sadykov, B.S. Balzhinimaev, T. Decamp, C. Mirodatos, Chem. Eng. Sci. 54 (1999) 4327.
[13] E.M. Sadovskaya, A.P. Suknev, L.G. Pinaeva, V.B. Goncharov, B.S. Balzhinimaev, C. Chupin, C. Mirodatos, J. Catal. 201 (2001) 159.
[14] A.Y. Stakheev, C.W. Lee, S.J. Park, P.J. Chong, Catal. Lett. 38 (1996) 271.
[15] M.C. Campa, S. De Rossi, G. Ferraris, V. Indovina, Appl. Catal. B: Env. 8 (1996) 315.
[16] E.M. Sadovskaya, A.P. Suknev, L.G. Pinaeva, V.B. Goncharov, B.S. Balzhinimaev, C. Chupin, J. Pérez-Ramirez, C. Mirodatos, J. Catal. 225 (2004) 179.
[17] J.H. Scofield, J. Electron Spectrosc. Relat. Phenom. 8 (1976) 129.
[18] S. Lars, T. Anderson, R.F. Howe, J. Phys. Chem. 93 (1989) 4913.
[19] L. Guczi, D. Bazin, Appl. Catal. A: Gen. 188 (1999) 163.
[20] T.J. Chuang, C.R. Brundle, D.W. Rice, Surf. Sci. 59 (1976) 413.
[21] Z. Zsoldos, L. Guczi, J. Phys. Chem. 96 (1992) 9393.
[22] G. Fierro, M.A. Eberhardt, M. Houalla, D.M. Hercules, W.K. Hall, J. Phys. Chem. 100 (1996) 8468.
[23] J. Yan, M.C. Kung, W.M.H. Sachtler, H.H. Kung, J. Catal. 172 (1997) 178.
[24] Y. Li, J.N. Armor, Appl. Catal. B: Env. 5 (1995) L257.
[25] Y. Li, J.N. Armor, Appl. Catal. B: Env. 3 (1993) L1.
[26] M. Mhamdi, E. Marceau, S. Khaddar-Zine, A. Ghorbel, M. Che, Y. Ben Taarit, F. Villain, Catal. Lett. 98 (2004) 135.
[27] D. Kaucky, A. Vondrova, J. Dedecek, B. Wichterlova, J. Catal. 194 (2000) 318.
[28] M. Iwamoto, H. Hamada, Catal. Today 10 (1991) 57.
[29] B. Wichterlova, J. Dedecek, Z. Sobalik, A. Vondrova, K. Klier, J. Catal. 169 (1997) 194.
[30] P. Budi, R.F. Howe, Catal. Today 38 (1997) 175.
[31] V.A. Sadykov, S.A. Beloshapkin, E.A. Paukshtis, G.M. Alikina, D.I. Kochubei, S.P. Degtyarev, N.N. Bulgakov, S.A. Veniaminov, E.V. Netyaga, E.V. Bunina, A.N. Kharlanov, E.V. Lunina, V.V. Lunin, V.A. Matyshak, A.Y. Rozovskii, Polish J. Env. Stud. 1 (1997) 21.
[32] P. Arnoldy, J.A. Moulijn, J. Catal. 93 (1985) 38.
[33] A.D. Cowan, N.W. Cant, B.S. Haynes, P.F. Nelson, J. Catal. 176 (1998) 329.
[34] Y. Li, J. Battavio, J.N. Armor, J. Catal. 142 (1993) 561.
[35] A.S. Lermontov, J.S. Girardon, A. Griboval-Constant, S. Pietrzyck, A.Y. Khodakov, Catal. Lett. 101 (2005) 117.
[36] Y. Schuurman, A.C. van Veen, C. Chupin, C. Mirodatos, Top. Catal. 2006, in press.